Low-field magnetic properties of $CoCl_2$-graphite intercalation compounds

1990 J. Phys.: Condens. Matter 2 8391

(http://iopscience.iop.org/0953-8984/2/42/016)

J. Phys.: Condens. Matter 2 (1990) 8391–8404. Printed in the UK

Low-field magnetic properties of $CoCl_2$–graphite intercalation compounds

J T Nicholls†§ and G Dresselhaus‡

† Department of Physics, Massachusetts Institute of Technology, Cambridge, MA 02139, USA

‡ Francis Bitter National Magnet Laboratory, Massachusetts Institute of Technology, Cambridge, MA 02139, USA

Received 24 July 1990

Abstract. We report low-field (0–1200 Oe) magnetic properties of the $CoCl_2$–graphite intercalation compounds (GIC). Using high-quality stage-1 $CoCl_2$–GIC samples, we determine that there is only one low-temperature field-induced transition at $H_t(0) = 380$ Oe in these compounds. We estimate that the interplanar exchange interaction $J' = 0.025$ K, and hence the interlayer-to-intralayer exchange coupling ratio is $|J'/J| \sim 10^{-3}$ for the stage-1 $CoCl_2$–GIC. The H_t–T phase diagram for the stage-1 $CoCl_2$–GIC has been mapped out using both in-plane susceptibility χ' and c-axis resistivity ρ_c measurements. No field-induced transition in the susceptibility that could be ascribed to the presence of a sixfold in-plane anisotropy field H_6 was observed. Zero-field susceptibility $\chi = \chi' - i\chi''$ measurements on $CoCl_2$ intercalation compounds with larger c-axis repeat distances than the stage-1 compounds showed one maximum in the real component $\chi'(T)$ at T_{max}, and two maxima in the imaginary component $\chi''(T)$ at T_{cl} and T_{cu}, where $T_{cl} < T_{max} < T_{cu}$. Additionally, the magnitude of the $\chi'(T)$ maximum at T_{max} is approximately 10–15 times greater than the magnitude of the maxima in $\chi''(T)$. For the stage-2 compounds we obtain $|J'/J| \sim 10^{-4}$, representing an order of magnitude decrease with respect to the stage-1 compound.

1. Introduction

When intercalated into graphite, the Cl^-–Co^{2+}–Cl^- layered sandwich structure of pristine $CoCl_2$ is preserved [1]. Each $CoCl_2$ tri-layer sandwich is separated from other $CoCl_2$ sandwiches by n graphene planes, where n denotes the stage index of the resulting graphite intercalation compound (GIC). The main interest in $CoCl_2$–GIC has been the possibility of reducing the interlayer antiferromagnetic interaction J', by increasing the magnetic interlayer separation through intercalation. Work on these compounds was motivated by the idea that if J' is decreased sufficiently, the strong ferromagnetic in-plane interactions will dominate and give rise to a two-dimensional (2D) magnetic phase transition.

From high-field magnetization [2] and high-temperature DC magnetic susceptibility [3] measurements, the $CoCl_2$–GIC are known to exhibit strong XY spin anisotropy. That is, at low temperatures, the Co^{2+} spins point within the xy plane. The similarity

§ Present address: Cavendish Laboratory, Madingley Road, Cambridge CB3 0HE, UK.

0953-8984/90/428391+14$03.50

of the $CoCl_2$ sandwich structures in pristine $CoCl_2$ and the $CoCl_2$–GIC, and the XY spin anisotropy exhibited by both types of $CoCl_2$ compounds, provide strong evidence that the anisotropic magnetic Hamiltonian introduced by Lines [4] for pristine $CoCl_2$

$$\mathcal{H}_{CoCl_2} = -J \sum_{i>j} \boldsymbol{S}_i \cdot \boldsymbol{S}_j + J_A \sum_{i>j} S_{iz} S_{jz} + J' \sum_{i>k} \boldsymbol{S}_i \cdot \boldsymbol{S}_k - J'_A \sum_{i>k} S_{iz} S_{kz} \tag{1}$$

is also applicable to the $CoCl_2$–GIC. The low-temperature magnetic ground state of $CoCl_2$ consists of ferromagnetically aligned sheets of Co^{2+} spins that are stacked in an antiferromagnetic arrangement along the c-axis [5].

The stage-1 $CoCl_2$–GIC have been extensively studied, and information concerning the dependence of $J'_{\text{stage-1}}$ on the interlayer separation has been obtained via low-temperature magnetic measurements performed under pressure [6].

In this paper we present magnetic results for $CoCl_2$–GIC with stages 1 through 3, as well as measurements on a $CoCl_2/AlCl_3$ bi-intercalation compound. The aim of this study is to investigate the effect of reducing J' as the interlayer spacing I_c is increased. The remainder of this paper is arranged as follows. In section 2 we briefly summarize the reaction conditions used to prepare the various samples investigated in this work. The following section, section 3, presents the magnetic results that are discussed in section 4.

2. Sample preparation and characterization

All the $CoCl_2$–GIC investigated in this paper were synthesized using a single-zone intercalation reaction. In such a reaction the graphite pieces and some pristine anhydrous $CoCl_2$ powder are placed at separate ends of a glass ampoule, which is then sealed containing a known pressure of dry chlorine gas. Of the different $CoCl_2$–GIC, we found it easiest to prepare the stage-1 compounds, using high chlorine pressure (2–3 atm chlorine pressure at room temperature) and high reaction temperatures (660°C). These extreme reaction conditions ensure that complete intercalation takes place, and it is unlikely that high-stage impurity phases exist within the stage-1 $CoCl_2$–GIC samples. Stage-1 samples were synthesized from kish graphite and highly oriented pyrolytic graphite (HOPG) with equal success, giving a c-axis repeat distance of $I_c = 9.38 \pm 0.02$ Å. The stage-2 $CoCl_2$–GIC were synthesized at 560°C using a room temperature chlorine pressure of 600 torr. The synthesis conditions for preparing higher stage ($n > 2$) $CoCl_2$–GIC are not well established. We prepared stage-3 $CoCl_2$–GIC samples using a room temperature chlorine pressure of about 500 torr, and a reaction temperature of 560°C. However, it should be mentioned that sometimes we obtained stage-2, stage-3, and mixed stage-2/stage-3 $CoCl_2$–GIC samples all within the same reaction ampoule. From entropy considerations there is an increased chance of impurity stages existing in higher stage compounds, and elastic neutron scattering measurements of a nominal stage-2 $CoCl_2$–GIC revealed a large ($\sim 30\%$) concentration of admixed stages [7]. With the above considerations in mind, we show in figure 1 the x-ray diffraction scan of a stage-3 $CoCl_2$–GIC. From the indexed (00ℓ) Bragg peaks, we determine the c-axis repeat distance to be $I_c = 16.02 \pm 0.10$ Å.

Due to the difficulty in preparing homogeneous high-stage $CoCl_2$–GIC samples, bi-intercalation compounds have been investigated as alternative systems for observing quasi-two-dimensional magnetic behaviour. To synthesize $CoCl_2$ bi-intercalation compounds, a stage-2 (or higher) $CoCl_2$–GIC sample is required as starting material for a

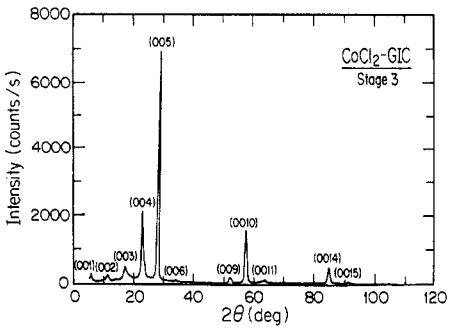

Figure 1. The (00ℓ) x-ray diffraction pattern, using Cu Kα radiation, of a stage-3 $CoCl_2$–GIC. From the indexed Bragg peaks, we determine the c-axis repeat distance to be $I_c = 16.02 \pm 0.10$ Å.

second intercalation reaction, where the non-magnetic second intercalate is introduced between the remaining adjacent graphene layers.

The bi-intercalation compounds investigated here were synthesized using $AlCl_3$ as the second intercalate; $AlCl_3$ is less toxic and less volatile than $GaCl_3$ that was used to synthesize earlier bi-intercalation compounds [8]. The intercalation of $AlCl_3$ was carried out using a two-zone reaction for two days with 1 atm of chlorine. The $AlCl_3$ end of the ampoule was heated to 150°C, while the stage-2 sample was heated about 10°C higher using a small heating tape. These particular reaction conditions were chosen after we had investigated the conditions for synthesizing pure stage-1 $AlCl_3$-GIC from HOPG and kish graphite, and the synthesis conditions quoted above gave non-violent reactions and yielded samples that were saturated with intercalate and blue in colour (indicating stage-1). It is very important that the second intercalation reaction proceeds smoothly, otherwise the $AlCl_3$ will displace the $CoCl_2$ from the stage-2 $CoCl_2$–GIC.

The main advantage of using $AlCl_3$ for the second intercalation is that, upon exposure to the water vapour in air, the $AlCl_3$ bi-intercalation samples are more chemically stable than their $GaCl_3$ counterparts. Therefore, the $CoCl_2/AlCl_3$ compound is easily handled in a glove-bag, and there is little degradation of the sample when it is briefly exposed to air during transfer from the glove-bag to the susceptibility probe.

The interplanar repeat distances I_c of the various $CoCl_2$ compounds are summarized in table 1.

Table 1. Structural and magnetic properties of various $CoCl_2$–GIC.

	I_c(Å)	$T_{c\,l}$(K)[a]	T_{max}(K)[b]	$T_{c\,u}$(K)[a]
Stage-1	9.38	—	$T_{c2} = 9.7$	—
Stage-2	12.70	7.8	8.6	9.2
Stage-3	16.02	7.7	8.4	9.5
Bi-stage-2[c]	19.1	7.4	8.1	9.2

[a] From the peak in $\chi''(T)$.
[b] From the peak in $\chi'(T)$.
[c] Stage-2 $CoCl_2/AlCl_3$–GIC.

3. Magnetic results for $CoCl_2$–GIC

Measurements of the in-plane AC susceptibility $\chi = \chi' - i\chi''$, where χ' and χ'' are the real and imaginary components, respectively, were performed using a set-up similar to that described previously [9]. In-plane resistance measurements were carried out using the standard four-probe technique, with applied currents kept below 1 mA to reduce sample heating. For measurements requiring a magnetic field, the field $\boldsymbol{H}$ was applied within the xy plane of the GIC sample, perpendicular to the c-axis.

Using the convention of earlier papers in the field, we define the lower and upper transition temperatures of the stage-1 $CoCl_2$–GIC to be T_{c1} and T_{c2}, respectively. For higher stage ($n \geq 2$) compounds, the lower transition temperature is labelled T_{cl}, and the upper transition temperature is labelled T_{cu}. For all stages, the temperature of the maximum in the real part of the susceptibility is defined to be T_{max}.

The magnetic results are presented in an order determined by increasing interplanar repeat distance and hence decreasing interplanar exchange interaction.

3.1. Stage-1 $CoCl_2$–GIC

The zero-field susceptibility $\chi'(T)$ of a stage-1 $CoCl_2$–GIC is shown in figure 2, and exhibits a maximum at $T_{max} = T_{c2} = 9.7$ K. This temperature is identified to be close to the Néel temperature T_N, and elastic neutron scattering measurements of Ikeda *et al* [10] confirm that there is long-range antiferromagnetic order below this temperature. As the temperature is lowered through T_N, the ferromagnetically aligned spins within each magnetic layer become ordered into an antiferromagnetic arrangement of sheets of spins stacked along the c-axis. The lower peak in $\chi'(T)$, defined to be the transition temperature $T_{c1} = 8.6$ K, has also been observed by Yazami and Chouteau [11]. The imaginary component of the zero-field susceptibility $\chi''(T)$ exhibits [6] a single peak at T_{c2}.

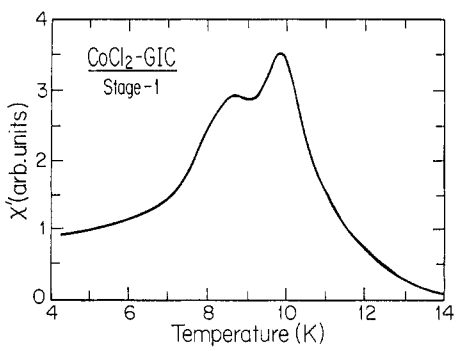

Figure 2. The zero field in-plane susceptibility $\chi'(T)$ of a stage-1 $CoCl_2$–GIC. The upper and lower peaks are at temperatures T_{c2} and T_{c1}, respectively. The upper transition T_{c2} is identified to be just below the Néel temperature T_N, whereas the physical origin of the transition at T_{c1} has not yet been explained.

In-plane susceptibility $\chi'(H)$ measurements at constant temperature of a stage-1 $CoCl_2$–GIC are shown in figure 3. At low temperatures (curve (a)), the field-induced peak defining H_t occurs at 380 Oe. As the temperature is raised, this peak at H_t first becomes sharper and stronger in magnitude (traces (b)–(d)) up to ~ 8.8 K and

then decreases in intensity (traces (*e*) and (*f*)) and finally disappears at ~10 K, a temperature about 0.3 K above T_{c2}. The inset of figure 3 shows the magnitude of the susceptibility peak $\chi'(H_t)$ against temperature, showing that the peak in $\chi'(H_t)$ occurs close to T_{c1}. The values of H_t are plotted as a function of temperature in figure 4.

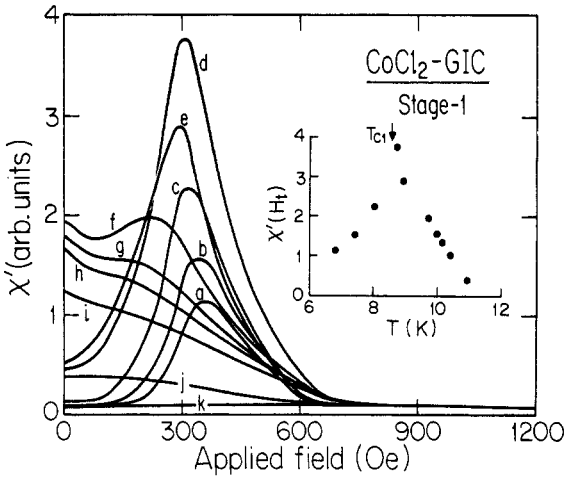

Figure 3. The in-plane susceptibility $\chi'(H)$ of stage-1 $CoCl_2$-GIC at temperatures (*a*) 6.80, (*b*) 7.41, (*c*) 8.02, (*d*) 8.70, (*e*) 8.90, (*f*) 9.72, (*g*) 10.00, (*h*) 10.14, (*i*) 10.41, (*j*) 10.93, and (*k*) 13.40 K. The inset shows the magnitude of the susceptibility peak $\chi'(H_t)$ for various temperatures. The peak $\chi'(H_t)$ shown in the inset occurs within experimental error of the value of T_{c1} shown by the arrow as determined from the temperature scan in figure 2.

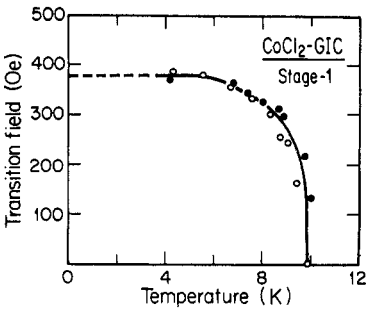

Figure 4. The $H_t - T$ phase diagram of stage-1 $CoCl_2$-GIC. The full circles (●) are derived from the peak in the $\chi'(H)$ traces of figure 3, and the open circles (○) are obtained from the maximum value of the derivatives $|\partial\rho_c(H)/\partial H|$ of the scans in figure 8. The full line is a guide to the eye.

Earlier low-temperature measurements [12] of $\chi'(H)$ for stage-1 $CoCl_2$-GIC showed two field-induced transitions; however, based on experience from measurements of many stage-1 $CoCl_2$-GIC samples, and the observation of similar effects in stage-1 $NiCl_2$-GIC [13] and stage-1 $Co_xMg_{1-x}Cl_2$-GIC [14], it is now believed that the transition reported at lower field is not associated with stage-1 and that high-quality stage-1 $CoCl_2$ and $NiCl_2$ samples show only one, clear, field-induced peak at H_t.

If the field-induced transition at H_t is first-order, its width is expected to be proportional to $\lambda\Delta M$, where ΔM is the size of the magnetization jump at the transition, and λ is the demagnetization factor of the sample. The demagnetization factor λ can be estimated, assuming that the sample is ellipsoidal in shape, using the published tables of Osborn [15]. Curve (a) of figure 5 shows the $\chi'(H)$ trace at $T = 4.2$ K for a sample with demagnetization factor $\lambda = 0.88$; the full width at half maximum (FWHM) of the transition at H_t is estimated to be 120 Oe. A susceptibility trace, at the same temperature, for a sample with $\lambda = 3.2$ (labelled (b) in figure 5) has a field width of 400 Oe. Assuming that ΔM is the same for both samples, the transition widths for these two samples approximately scale with λ, as predicted for a first-order phase transition at H_t. This suggests two possible interpretations of the magnetic phase diagrams. In the first case, H_t is a spin flop transition; however, the spin flop to paramagnetic transition at higher field values has not been detected up to a field of 1 T. In the second interpretation, H_t is the only transition in an applied field, and the stage-1 $CoCl_2$–GIC system is a metamagnet. Our measurements suggest that the latter possibility is more likely, and other measurements, for example, neutron scattering at low temperatures confirm [16] that, in the stage-1 $CoCl_2$–GIC, there is a loss of c-axis antiferromagnetic order near ~380 Oe.

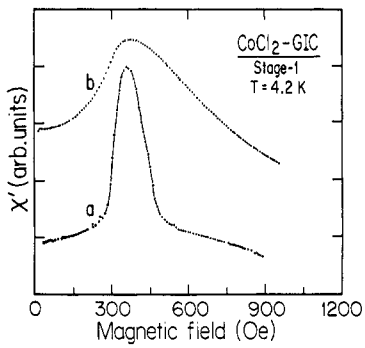

Figure 5. Traces of the field-dependent susceptibility $\chi'(H)$ at $T = 4.2$ K for two stage-1 $CoCl_2$–GIC samples with estimated demagnetization factors of (a) 0.88 and (b) 3.2.

The peak at H_t has been identified by elastic neutron scattering [16] to be the magnitude of the applied magnetic field that just overcomes the c-axis antiferromagnetic order. We can therefore estimate J' from the relation

$$J' = g_\perp \mu_B H_t / 2zS. \tag{2}$$

Inserting the appropriate values for $g_\perp = 6$, and $z = 6$ for the number of nearest-neighbour spins on the adjacent spin planes, we obtain the numerical relation $J'(\mathrm{K}) = 6.7\times10^{-5} H_t(\mathrm{Oe})$. Hence, from the extrapolation of $H_t(T)$ to low temperature $H_t(0) =$ 380 Oe, we calculate the interlayer coupling to be $J' = 0.025$ K for the stage-1 $CoCl_2$–GIC.

In-plane resistivity $\rho_a(T)$ measurements [17] provide another method for observing the antiferromagnetic ordering temperature T_N of the stage-1 $CoCl_2$–GIC. The zero-field resistivity $\rho_a(T)$ increases sharply and anomalously as T is lowered below T_N

(see figure 6*a*) whereas the resistivity behaviour for $T \gg T_N$ is similar to that for non-magnetic acceptor GIC [18]. The expression 'anomalous' refers to the observation that the scattering (and hence the resistivity) is enhanced in the ordered magnetic phase; the opposite behaviour (reduced resistivity below T_N) is usually observed in conducting antiferromagnetic materials. This anomalous increase in $\rho_a(T)$ below T_N has been identified with an additional scattering effect arising from a Fermi surface modified by *c*-axis zone-folding due to the antiferromagnetic stacking of the ferromagnetically ordered spin planes [19]. The long-range coherence of this antiferromagnetic stacking along the *c*-axis in the stage-1 $CoCl_2$–GIC has been established by magnetic neutron scattering [10]. Temperature sweeps of $\rho_a(T)$ in an applied magnetic field H (see figures 6(*b*)–(*f*)) show that H reduces the antiferromagnetic order and thus suppresses the anomalous increase in the resistivity below T_N.

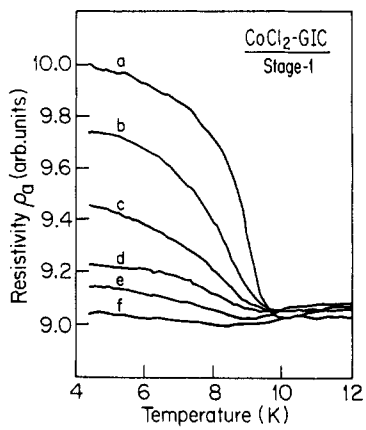

Figure 6. The in-plane resistivity $\rho_a(T)$ of a stage-1 $CoCl_2$–GIC sample measured in applied in-plane magnetic fields of (*a*) 0, (*b*) 450, (*c*) 600, (*d*) 900, (*e*) 1000, and (*f*) 1200 Oe.

Figure 7 shows *c*-axis resistivity $\rho_c(T)$ behaviour that exhibits the same temperature-dependent features as the $\rho_a(T)$ data shown in figure 6. The $\rho_c(T)$ behaviour for a similar stage-1 sample was confirmed [20] independently using a more elaborate measurement system, which ensures that the current flows parallel to the *c*-axis throughout the sample. Figure 8 shows $\rho_c(H)$ data that exhibit the same field-dependent behaviour as $\rho_a(H)$. The values of H_t, determined from the maximum of the derivative $|\partial\rho_c(H)/\partial H|$, are plotted as open circles (O) in figure 4 for various temperatures. The close agreement of $H_t(T)$, as determined from susceptibility and transport measurements, gives strong support for the theory proposed by Sugihara *et al* [19]. This theory proposes that the band gaps at the Fermi surface associated with the antiferromagnetic ordering enhances the electron scattering in the magnetic state. This scattering channel is quenched in a magnetic field which eliminates the antiferromagnetic state.

Some doubt has been raised [13] as to whether domains and staging defects introduced by the intercalate layer could cause leakage of ρ_a into ρ_c. The mixing of ρ_a and ρ_c is a serious concern in transport investigations of any highly anisotropic material. The magnitude of the anomaly below T_N shown in figure 7

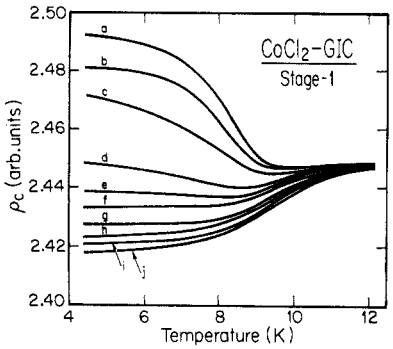

Figure 7. The c-axis resistivity $\rho_c(T)$ of a stage-1 $CoCl_2$-GIC measured in applied in-plane magnetic fields of (*a*) 0, (*b*) 300, (*c*) 375, (*d*) 600, (*e*) 675, (*f*) 750, (*g*) 900, (*h*) 990, (*i*) 1125, and (*j*) 1200 Oe.

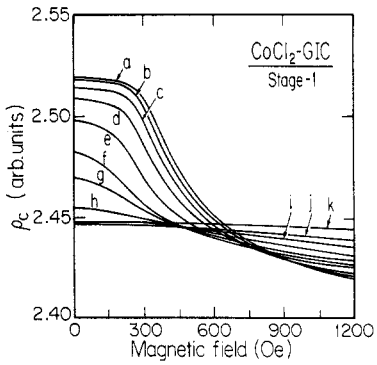

Figure 8. The c-axis resistivity $\rho_c(H)$ of a stage-1 $CoCl_2$-GIC measured at temperatures (*a*) 4.3, (*b*) 5.55, (*c*) 6.68, (*d*) 7.56, (*e*) 8.34, (*f*) 8.75, (*g*) 9.05, (*h*) 9.40, (*i*) 9.87, (*j*) 10.28, and (*k*) 11.55 K.

is $[\rho_c(0) - \rho_c(T_N)]/\rho_c(0) = \Delta\rho_c/\rho_c \approx 4\%$ ($\Delta\rho_c/\rho_c \approx 8\%$ was measured [20] on another sample) is slightly smaller than the anomaly observed in the in-plane resistivity $\Delta\rho_a/\rho_a \approx 10\%$ (see figure 6 and [17]). At this time, we are not sure whether the resistivity anomalies in $\rho_a(T)$ and $\rho_c(T)$ are both intrinsic effects, or whether in a 'perfect' sample the anomaly is present in only one of the resistivity configurations.

3.2. Stage-2 $CoCl_2$-GIC

The real and imaginary components of the zero-field susceptibility of our stage-2 $CoCl_2$-GIC have been published in a recent paper [6]. The real component $\chi'(T)$ exhibits a maximum at $T_{max} = 8.6$ K, whereas $\chi''(T)$ shows peaks at $T_{cl} = 7.8$ K and $T_{cu} = 9.2$ K. In the low-temperature scans of $\chi'(H)$ for the stage-2 $CoCl_2$-GIC, a weak shoulder is observed at ~10–15 Oe [21]. Figure 10 shows the position of this weak feature as a function of temperature; the anomaly is found to disappear at 9.1 K. A similar low-temperature transition at $H_t = 12$ Oe has also been observed at 6 K in the field scan of the $(00\frac{1}{2})$ magnetic neutron scattering [22] Bragg peak and this is plotted as an open circle (○) in figure 9. Suzuki *et al* [22] suggest that H_t is a spin flop transition. However, we could find no evidence for a spin flop to paramagnetic

transition at higher field values, and we shall assume that H_t is the magnetic field at which the c-axis antiferromagnetic order is overcome. Whichever of the two explanations is correct, the transition at H_t is a consequence of three-dimensional (3D) antiferromagnetic order, and the antiferromagnetic interplanar exchange parameter in the stage-2 compound $J'_{\text{stage-2}}$ is an order of magnitude smaller than $J'_{\text{stage-1}}$.

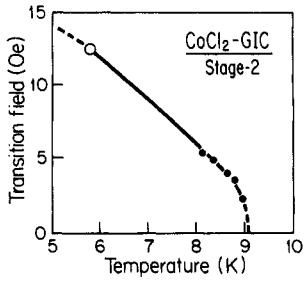

Figure 9. The temperature dependence of the field anomaly H_t in a stage-2 $CoCl_2$–GIC sample. The low-temperature point, denoted by an open circle (O), is the result obtained from neutron scattering [22].

Due to variability in the samples, neutron studies of stage-2 $CoCl_2$–GIC have observed different transition temperatures, for example $T_{cl} = 8.8$ K, $T_{cu} = 9.4$ K by one group [7], and $T_{cl} = 8.0$ K, $T_{cu} = 9.1$ K by another group [22]. From neutron scattering measurements, it is desirable to measure the temperature dependence of the $(00\frac{1}{2})$ magnetic Bragg peak, and thus determine the temperature at which 3D antiferromagnetic order disappears. In experimental studies of stage-2 $CoCl_2$–GIC [7, 10], there is a monotonic decrease of the intensity of the $(00\frac{1}{2})$ peak when the temperature is raised from liquid-helium temperatures. As the temperature approaches 8 K, the exact position at which the intensity of the $(00\frac{1}{2})$ peak goes to zero is complicated by the presence of a large background tail. Neutron scatterers have identified this tail with diffuse scattering from 2D ferromagnetic spin correlations, and by careful separation of this diffuse scattering from the $(00\frac{1}{2})$ peak, it appears that the 3D antiferromagnetic order disappears near 9.0 K [7]. Wiesler *et al* [7] state that the 3D ordering temperature occurs at the lower transition $T_{cl} = 8.8$ K. It should be added that the tail could be also caused by smearing of the 3D transition, as is observed in stage-1 $CoCl_2$–GIC [10], or by the presence of impurity stages.

In our study of stage-2 $CoCl_2$–GIC, our samples are prepared slightly differently and are thus expected to exhibit different transition temperatures. Indeed, the transition temperatures of our stage-2 samples listed in table 1 are slightly different from those quoted from other research groups in the previous paragraph. From figure 9, we see that the field structure disappears at a temperature that is closer to T_{cu} rather than T_{cl}, where the two transition temperatures have been determined from the imaginary component of the susceptibility [6]. Therefore, in contradiction to Wiesler *et al* [7] we observe the 3D magnetic order to disappear close to the upper transition temperature T_{cu}.

Although small anomalous effects have been seen [17] near T_{cu} in the $\rho_a(T)$ curves of stage-2 $CoCl_2$–GIC, attributed to spin-disorder scattering as the magnetic phase is established, no such features were observed in $\rho_c(T)$.

3.3. Stage-3 $CoCl_2$-GIC

The real and imaginary components of the zero-field susceptibility of a stage-3 $CoCl_2$–GIC are shown in figure 10(*a*). The features are similar to the stage-2 results; $\chi'(T)$ has one peak at T_{max}, whereas $\chi''(T)$ exhibits peaks at $T_{cl} = 7.7$ K and $T_{cu} = 9.5$ K. The position T_{cu} of the upper peak in $\chi''(T)$ coincides with a weak shoulder that can be seen in the real part of the susceptibility $\chi'(T)$. In an earlier study [23] of a stage-3 $CoCl_2$–GIC, this shoulder in $\chi'(T)$ has been claimed to be the upper transition T_{cu}.

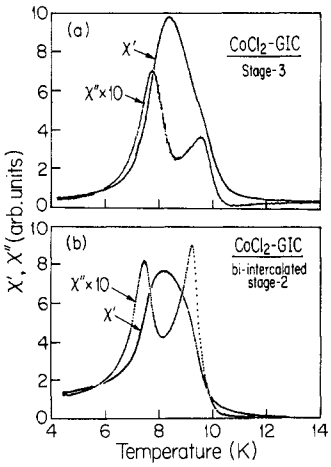

Figure 10. The susceptibility $\chi(T) = \chi'(T) - i\chi''(T)$ of (*a*) stage-3 $CoCl_2$–GIC, and (*b*) stage-2 $CoCl_2$–GIC bi-intercalated with $AlCl_3$. The real component of the susceptibility exhibits a peak at T_{max}, whereas the imaginary component χ'' x 10 exhibits peaks at T_{cl} and T_{cu}.

Low temperature scans of $\chi'(H)$ revealed no low-field structure.

3.4. Bi-intercalated stage-2 $CoCl_2$-GIC

The traces of the zero-field susceptibility $\chi'(T)$ and $\chi''(T)\times 10$ are shown in figure 10(*b*) for a stage-2 $CoCl_2$–GIC bi-intercalated with $AlCl_3$. As in figure 10(*a*) the position T_{cu} of the upper peak in $\chi''(T)$ appears at a temperature that coincides with a weak shoulder that can be seen in the real part of the susceptibility $\chi'(T)$. Again, the relative positions of the transition temperatures are similar to those observed in the stage-2 $CoCl_2$–GIC.

If the bi-intercalated sample is prepared carefully, the total number of Co^{2+} ions, and their distribution on the magnetic layers, will remain unchanged by the introduction of $AlCl_3$. Figure 11 shows the susceptibility of a stage-2 $CoCl_2$–GIC (*a*) before, and (*b*) after bi-intercalation. The original stage-2 sample was found to contain some impurities (not seen in the (00ℓ) x-ray diffraction scan) that give rise to a bump in the susceptibility at 9.3 K. However, after bi-intercalation, two features in $\chi'(T)$ are clear. First, the magnitude of the susceptibility in the bi-intercalation compound is greater for the same number of Co^{2+} ions, thereby providing strong evidence for the increasing two-dimensionality of the magnetism as a result of the intercalation of the non-magnetic $AlCl_3$. Second, the susceptibility peak in $\chi'(T)$ shifts from 8.4 to 8.1 K after the intercalation with $AlCl_3$. This decrease in T_{max} is in agreement with the earlier work of Rosenman *et al* [8] on stage-2 $CoCl_2$–GIC bi-intercalated with $GaCl_3$.

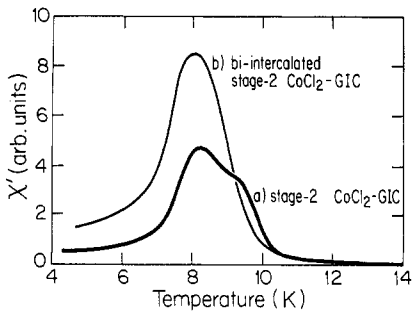

Figure 11. The real component of the in-plane susceptibility $\chi'(T)$ of a stage-2 $CoCl_2$–GIC (*a*) before and (*b*) after bi-intercalation with $AlCl_3$.

4. Summary and discussion

When comparing results from different research groups we should be aware of the variation in the magnetic properties of samples with the same nominal stage. Variations in the in-plane filling factor may give rise to variations of the observed transition temperatures, as has been demonstrated in the study [14] of the dilution of the magnetic properties of stage-1 $CoCl_2$–GIC with Mg^{2+} ions. Similar dilution of the magnetic properties of the higher stage compounds is also expected.

The magnetic properties of the $CoCl_2$–GIC become more two-dimensional in the higher stage compounds where the magnetic layers are separated from each other by additional graphene layers. This increasing two-dimensionality is reflected in the increasing strength of χ_{max}, the magnitude of the susceptibility (per Co^{2+} ion), as we progress to higher stages [24]. This is most clearly seen in the traces (see figure 11) of the real part of the susceptibility shown (*a*) before and (*b*) after bi-intercalation with $AlCl_3$.

The $CoCl_2$–GIC have been investigated by many experimental techniques, as reviewed [25, 26] recently, and many of the conclusions concerning the magnetic properties of the $CoCl_2$–GIC are applicable to the $NiCl_2$–GIC.

4.1. Stage-1 $CoCl_2$-GIC

Experimentally, the results presented in section 3.1 show that the AC susceptibility $\chi(H,T)$ and the resistivity measurements, $\rho_a(H,T)$ and $\rho_c(H,T)$, give a consistent picture of the magnetic phase transitions in the stage-1 $CoCl_2$–GIC compounds. Stage-1 $CoCl_2$–GIC are quasi-2D magnetic systems with an interlayer-to-intralayer exchange coupling ratio of $|J'/J| \sim 10^{-3}$. These system order into a long-range antiferromagnetic arrangement of stacked ferromagnetic sheets at a Néel temperature T_N just above $T_{c2} = 9.7$ K. The nature of the transition at $T_{c1} = 8.6$ K, observed in susceptibility measurements by other groups, is still not understood and should be investigated by neutron scattering. Theoretically, it would appear that a model [19, 27] which incorporates zone-folding of the π-electron bands accounts for the resistivity anomalies in both $\rho_a(T)$ and $\rho_c(T)$, and can also qualitatively explain the magnetic field behaviour of $\rho_a(H)$ and $\rho_c(H)$.

In summary, the stage-1 magnetic results presented in this work and by other research groups [10, 16] are consistent; the stage-1 $CoCl_2$–GIC exhibit a clear 3D antiferromagnetic transition near 9.7 K. Stage-1 $CoCl_2$–GIC samples exhibiting [28] lower

Néel temperatures must have a lower intercalate filling factor that gives rise to diluted magnetic properties similar to those studied [14] in the stage-1 $Co_xMg_{1-x}Cl_2$–GIC.

4.2. Higher stage $CoCl_2$–GIC ($n \geq 2$)

In going from pristine $CoCl_2$ to stage-1 $CoCl_2$–GIC, there is a decrease in the interplanar antiferromagnetic exchange coupling J'. Such a decrease of J' is reflected in a reduction of the 3D ordering temperature T_N from 24.9 to 9.7 K [5]; in figure 12 we have plotted $\ln J'$ against $\ln T_N$ for these two compounds. Experimentally, the low-temperature phase of the stage-2 $CoCl_2$–GIC exhibits antiferromagnetic order with a short c-axis coherence length ξ_c = 22–70 Å(references 29,10 respectively). The limited size of ξ_c gives rise to low-temperature field-induced transitions that are very weak in magnitude in comparison to those observed in stage-1 $CoCl_2$–GIC. The lack of low-temperature long-range order could be attributed to the random stacking [1] of the intercalate layers in the stage-2 $CoCl_2$–GIC. Such random stacking gives rise to random fields that could disrupt the long-range antiferromagnetic c-axis order. From the low-temperature field structure at H_t =10–15 Oe, we can estimate (using equation (2)) the interlayer-to-intralayer exchange coupling ratio to be $|J'/J| \sim 10^{-4}$ for the stage-2 $CoCl_2$–GIC. The field structure in our stage-2 samples disappear at T = 9.1 K, which we define, for the purposes of figure 12, to be the Néel temperature of this compound. Our conclusion that, for a stage-2 $CoCl_2$–GIC, T_{cu} is a transition to long-range 3D order is in agreement with recent quasi-elastic neutron scattering data [30]. These latest data show that below T_{cu}, there is a component to the scattering due to long-range 2D magnetic order, such 2D order is a necessary condition for a transition to 3D long-range order that we have observed below T_{cu}.

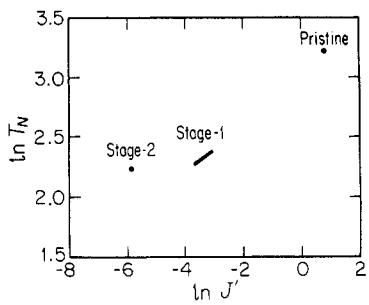

Figure 12. Plot of $\ln J'$ against $\ln T_N$ for pristine $CoCl_2$ [5], stage-1 [6], and stage-2 $CoCl_2$–GIC.

Low-temperature, field-induced structure has also been observed [31] in the in-plane susceptibility $\chi'(H)$ of stage-2 $NiCl_2$–GIC, in samples that exhibit two transitions at 17.3 and 19.4 K. The upper transition corresponds to our definition of T_{max}. At low temperatures and in an applied in-plane magnetic field, the stage-2 $NiCl_2$–GIC show a peak in $\chi'(H)$ at $\sim$ 35 Oe. As the temperature is increased, the field value of this peak in $\chi'(H)$ moves to lower fields; however, in a field sweep at 19.4 K (the highest temperature presented) there is still a clear maxima in $\chi'(H)$ at $\sim$ 15 Oe. Suzuki and Ikeda [31] report that this field structure persists up to 21.5 K. By comparison with our results for stage-2 $CoCl_2$–GIC, we would identify 21.5 K with the temperature at which 3D magnetic order disappears in stage-2 $NiCl_2$–GIC, that is T_{cu} = 21.5 K. This

identification is in rough agreement with the neutron scattering measurement [7] that shows that the integrated intensity of the $(00\frac{1}{2})$ Bragg peak disappears above 20 K in stage-2 $NiCl_2$–GIC.

Not included in figure 12 are data points for the stage-3 $CoCl_2$–GIC and the stage-2 $CoCl_2/AlCl_3$–GIC, as we have no estimate for J' or T_N of these compounds. In the stage-3 and bi-intercalated stage-2 $CoCl_2$–GIC, the magnitude of J' is expected to be further reduced.

The stage-3 $CoCl_2$–GIC and the bi-intercalated stage-2 $CoCl_2$–GIC exhibit temperature-dependent features that are similar to those observed in stage-2 $CoCl_2$–GIC. That is, the imaginary component of the temperature-dependent susceptibility $\chi''(T)$ exhibits two maxima at T_{cl} and T_{cu}, whereas the real part $\chi'(T)$ exhibits a maximum at T_{max}, where $T_{cl} < T_{max} < T_{cu}$. Additionally, the magnitude of the $\chi'(T)$ maximum at T_{max} is approximately 10–15 times greater than the magnitude of the maxima in $\chi''(T)$. The values of T_{cu}, T_{cl}, and T_{max} for the different stages and compounds are summarized in table 1. It is tempting to identify one of these temperatures as being the 2D magnetic Kosterlitz–Thouless (KT) transition. However, if the temperature T_{cu} is a transition to weak 3D magnetic order for all high-stage $CoCl_2$–GIC, then a search for a KT temperature should be conducted at higher temperatures.

It would be of interest to form bi-intercalation compounds of stage-3 $CoCl_2$–GIC and stage-2 $NiCl_2$–GIC.

Acknowledgments

This work was supported by National Science Foundation Grant (NSF) no DMR 88-19896. We are grateful to Professor M S Dresselhaus for her helpful comments and encouragement. HOPG was kindly supplied by Dr A W Moore of Union Carbide Corporation, and kish graphite was kindly provided by Professor H Suematsu of the University of Tokyo.

References

[1] Speck J S and Dresselhaus M S 1989 *Synth. Met.* **34** 211
[2] Nicholls J T, McNiff E J Jr and Dresselhaus G 1990 *Phys. Rev.* B **15** at press
[3] Wiesler, D G, Suzuki M, Chow P C and Zabel H 1986 *Phys. Rev.* B **34** 7951
[4] Lines M E 1963 *Phys. Rev.* **131** 546
[5] Hutchings M T 1973 *J. Phys. C: Solid State Phys.* **6** 3143
[6] Nicholls J T, Murayama C, Takahashi H, Mōri N, Tamegai T, Iye Y and Dresselhaus G 1990 *Phys. Rev.* B **41** 4953
[7] Wiesler D G, Suzuki M and Zabel H 1987 *Phys. Rev.* B **36** 7051
[8] Rosenman I, Batallan F, Simon Ch and Hachim L 1986 *J. Physique* **47** 1221
[9] Elahy M and Dresselhaus G 1984 *Phys. Rev.* B **30** 7225
[10] Ikeda H, Endoh Y and Mitsuda S 1985 *J. Phys. Soc. Japan* **54** 3232
[11] Yazami R and Chouteau G 1987 *Synth. Met.* **18** 543
[12] Szeto K Y, Chen S T and Dresselhaus G 1986 *Phys. Rev.* B **33** 3453
[13] Nicholls J T, Speck J S and Dresselhaus G 1989 *Phys. Rev.* B **39** 10047
[14] Nicholls J T and Dresselhaus G 1990 *Phys. Rev.* B **41** 9744
[15] Osborn J A 1945 *Phys. Rev.* **67** 351
[16] Chouteau G, Schweizer J, Tasset F and Yazami R 1988 *Synth. Met.* **23** 249
[17] Yeh N C, Sugihara K, Dresselhaus M S and Dresselhaus G 1989 *Phys. Rev.* B **40** 622
[18] Dresselhaus M S and Dresselhaus G 1981 *Adv. Phys.* **30** 139

[19] Sugihara K, Yeh N C, Dresselhaus M S and Dresselhaus G 1989 *Phys. Rev.* B **39** 4577
[20] Enoki T and Suzuki K 1989 private communication
[21] Chen S T 1985 Magnetic properties of graphite intercalation compounds *PhD Thesis* Massachusetts Institute of Technology
[22] Suzuki M, Ikeda H and Endoh Y 1983 *Synth. Met.* **8** 43
[23] Karaki Y, Tanaka N, Matsuura M, Murakami Y and Suzuki M 1986 *Extended Abstracts of the Symp. on Graphite Intercalation Compounds at the Materials Research Society Meeting, Boston* ed M S Dresselhaus, G Dresselhaus and S A Solin (Pittsburgh, PA: Materials Research Society Press) p 32
[24] Chen S T, Szeto K Y, Elahy M and Dresselhaus G 1984 *J. Chim. Phys.* **81** 863
[25] Dresselhaus G, Nicholls J T and Dresselhaus M S 1990 *Graphite Intercalation Compounds II* ed H Zabel and S A Solin (Berlin: Springer)
[26] Suzuki M 1990 *Magnetic Properties of Stage-2 $CoCl_2$-GICs (CRC Critical Reviews in Solid State and Material Science)* (Boca Raton, FL: Chemical Rubber Company)
[27] Sugihara K, Shiozaki I, Sampere S M, Suzuki M, Nicholls J T and Dresselhaus G 1989 *Synth. Met.* **34** 543
[28] Rogerie J, Simon Ch, Rosenman I, Vettier Ch, Godfrin H, Schweizer J, Vangelisti R, Pernot P and Perignon A 1989 *Synth. Met.* **34** 513
[29] Wiesler D G and Zabel H 1987 *Phys. Rev.* B **36** 7303
[30] Wiesler D G, Zabel H and Shapiro S M 1989 *Synth. Met.* **34** 505
[31] Suzuki M and Ikeda H 1981 *J. Phys. C: Solid State Phys.* **14** L923